Investigating the Influence of Synoptic-Scale Monsoonal Winds and Mesoscale Circulations on Diurnal Weather Patterns over Kenya Using a Mesoscale Numerical Model

JOSEPH R. MUKABANA

Department of Meteorology, University of Nairobi, Kenya

ROGER A. PIELKE

Department of Atmospheric Science, Colorado State University, Fort Collins, Colorado

(Manuscript received 1 March 1994, in final form 23 June 1995)

ABSTRACT

The Regional Atmospheric Modeling System (RAMS) developed at Colorado State University (CSU) was used to investigate the influence of the large-scale monsoonal winds and the mesoscale local circulations on the diurnal precipitation pattern over Kenya.

Three basic experiments were performed. In the first control experiment (CONTROL), RAMS was initialized using observational data ("variable initialization") from the global analyzed ECMWF 2.5° × 2.5° data of 0000 UTC 14 April 1985. The model was integrated forward in time for 24 h to simulate the large-scale flow fields over Kenya. Full physics including moist convection were implemented in the model. The model outputs were validated against available observations in order to determine the ability of the model in replicating the synoptic climatology prevailing over the study domain.

In the second experiment (MESO), the model simulation was started from an atmosphere at rest in order to exclude the large-scale flow from the model runs. This experiment used a horizontally homogeneous procedure to initialize the model. Moist convection was allowed to occur in the mesoscale simulations.

The third experiment (SYNO) excluded topography and land–water contrast data from the simulation. This was done in order to suppress the thermally induced local mesoscale circulations from the model runs so as to isolate and determine the role played by the synoptic-scale monsoonal winds on the generation of precipitation over Kenya. Topography was considered a local forcing that significantly modifies the large-scale temperature, moisture, and flow pattern.

Comparison was made between grid-averaged convective precipitation generated in the CONTROL, MESO, and SYNO simulations in order to identify the contribution of the synoptic-scale monsoonal flow and mesoscale circulations on the rainfall over Kenya.

Additional sensitivity experiments were performed to test the impact of topography and large water bodies on the precipitation over the country.

The results showed the following.

- More active convection developed in regions where the large-scale monsoonal winds in the lower troposphere converged with the local mesoscale circulations embedded in the large-scale flow.
- The large-scale flow advected substantially more moisture into the study domain as compared to the mesoscale flow alone. This illustrated the fact that monsoonal winds transport moisture from the Indian Ocean and advect it inland over the country.
- The large-scale monsoonal flow controlled the locations and movement of the convergence/precipitating zones over the country since the deep and active convective zones shifted in the direction of the prevailing low-level large-scale monsoonal flow.
- Topography has a significant impact on the diurnal precipitation pattern over the country. It generates anabatic–katabatic winds with a strong diurnal cycle; it modifies the large-scale temperature, moisture, and wind flow patterns over the country; and it also inhibits a substantial amount of the moisture-laden monsoonal winds from reaching farther inland over the country.
- The large water bodies (Lake Victoria, Lake Turkana, and the Indian Ocean) generate strong lake–land, sea–land-breeze circulations with an intense diurnal cycle that contributes to the overall precipitation pattern over the country.

It was concluded that the large-scale monsoonal winds and the mesoscale circulations are both crucial components in the realization of rainfall in Kenya during a wet season. The study similarly revealed the ability of the high-resolution RAMS model to replicate realistic meteorological fields for both large-scale and mesoscale weather systems in an equatorial regime.

1. Introduction

The monsoons may be defined as seasonal cross-equatorial winds that reverse direction with regularity

Corresponding author address: Dr. Roger A. Pielke, Department of Atmospheric Science, Colorado State University, Fort Collins, CO 80523.

and persistence every year. The causes of these winds can be attributed to the differential response of landmass and ocean to solar radiation. Most of the monsoon circulations are confined to the Tropics where the temperature contrast between land and ocean is sufficiently high to generate the circulations. Kenya is one of the land areas lying in the monsoon wind regime (Ramage 1971). The country sits astride the equator and is bounded by 4.5°N–5°S and 34°–42°E. It has an area of 582 646 km^2, comparable to the size of France or Texas.

Earlier studies have utilized mesoscale models to understand the strong local circulation systems and their influence on the weather over Kenya and the surrounding region (e.g., Fraederick 1972; Okeyo 1987). The contribution of the large-scale monsoonal flow, however, has not been given adequate attention in the few numerical studies carried out in this area. Nonetheless, various observational studies have shown that the diurnal variation of precipitation in east Africa is largely determined by the mesoscale flows, the synoptic-scale flows, and the interaction between the mesoscale and the synoptic-scale flows (Asnani and Kinuthia 1979; Asnani 1993). These studies assert that the synoptic-scale circulations interact with the local mesoscale systems to effect convergence zones and that the large-scale monsoonal winds control the intensity, movement, and locations of the convergence complexes and shower activity.

Kenya is subject to two monsoonal wind currents that are usually located over the ocean and are responsible for most of the seasonal weather observed over the country. The northeast (NE) monsoon airstream occurs during the Northern Hemisphere winter (December–January–February). The NE emanates from the Arabian anticyclone that is situated over the Arabian peninsula (Trewartha 1966; Findlater 1968). The NE follows a sea trajectory of only modest length. It is warm and dry. The southeast (SE) monsoonal current occurs in June–July–August and comes from the Mascarene anticyclone over the southern Indian Ocean. It is cool and moist. However, the SE monsoon air does not deposit any widespread rainfall over Kenya since it is subsident and diffluent over much of the country (Forsdyke 1949). March–May, the "long rains" season, and October–November and early December, the "short rains" season, constitute the two seasons associated with widespread rainfall over the country. During these two equinoctial seasons, there is increased surface heating; the ITCZ has its maximum influence over the country since the NE and the SE currents converge over Kenya and the surrounding region. The rainfall caused by the ITCZ over Kenya and other countries of east Africa has been documented by many investigators (e.g., Johnson 1962). In our study, we investigate the weather on an April day during the "long rains" season when rainfall was widespread over the country.

In this study an attempt was made to isolate the contribution of the large-scale monsoonal flow and the mesoscale circulations on the diurnal precipitation pattern over Kenya using the ECMWF pressure-level data together with the NMC rawinsonde and surface observations data sets of 14 April 1985. This date was picked because it had a fairly widespread rainfall over the country and displayed the average synoptic conditions reminiscent of a typical April weather situation.

Figure 1 shows the whole model domain, including Lake Victoria and the surrounding region. The physical features over Kenya together with the synoptic stations are illustrated in Fig. 1. Lake Victoria has an area of 68 400 km^2. This freshwater lake lies at 1132 m MSL in a depression between two highlands. It is the largest lake in the tropical region and has its own circulation pattern (Okeyo 1987). The topography used in the simulations is displayed in Fig. 2. The rectangle shown in Fig. 2 marks the approximate location of the Turkana–Marsabit "corridor" discussed in the text; this low-elevation region is associated with the low-level Turkana jet stream that occurs all year (Kinuthia 1992). The corridor is narrow at both the eastern entrance (area marked A in Fig. 2) and the western exit (area marked C) and broadens in the middle section (area marked B) where Lake Turkana (shown in Fig. 1), a body with alkaline waters, is located. Table 1 provides the definition of the symbols used in this study.

2. Synoptic climatology of the case study

The synoptic conditions of the case study prevailing at the start of the model simulations at 0000 UTC were characterized by southeasterly winds at the surface flowing in from the Mascarene anticyclone over Malagasy in the southwest Indian Ocean (see Fig. 3a). The surface winds attained a speed of 14 m s^{-1}. The wind field and geopotential on the 850-mb isobaric surface (Fig. 3b) showed southeast monsoonal winds over Kenya. However, there was a bifurcation of the wind over central and northwestern Kenya to central Africa. The two hemispheric monsoonal winds, the southeasterlies (SE), and the northeasterlies (NE) converged over the quasi-permanent near-equatorial trough (NET) that lies over the Indian Ocean off the coast of Somalia. The wind vectors and geopotential on the 700-mb isobaric surface (Fig. 3c) depicted a convergence of the two hemispheric monsoonal winds (the SE and the NE) over the eastern and northwestern part of the country including the adjacent Indian Ocean. This convergence zone marked the ITCZ position. The ITCZ is usually diffuse close to the surface over land in East Africa owing to high terrain elevations but manifests itself clearly between 750 and 700 mb (Kiangi et al. 1981). The monsoonal wind vectors over Kenya at the 500-mb level (figure not shown) displayed a northwesterly flow over the country. The geopotential field at 500-mb showed a substantial tilt of the subtropical ridge equatorward with the attendant westerly flow

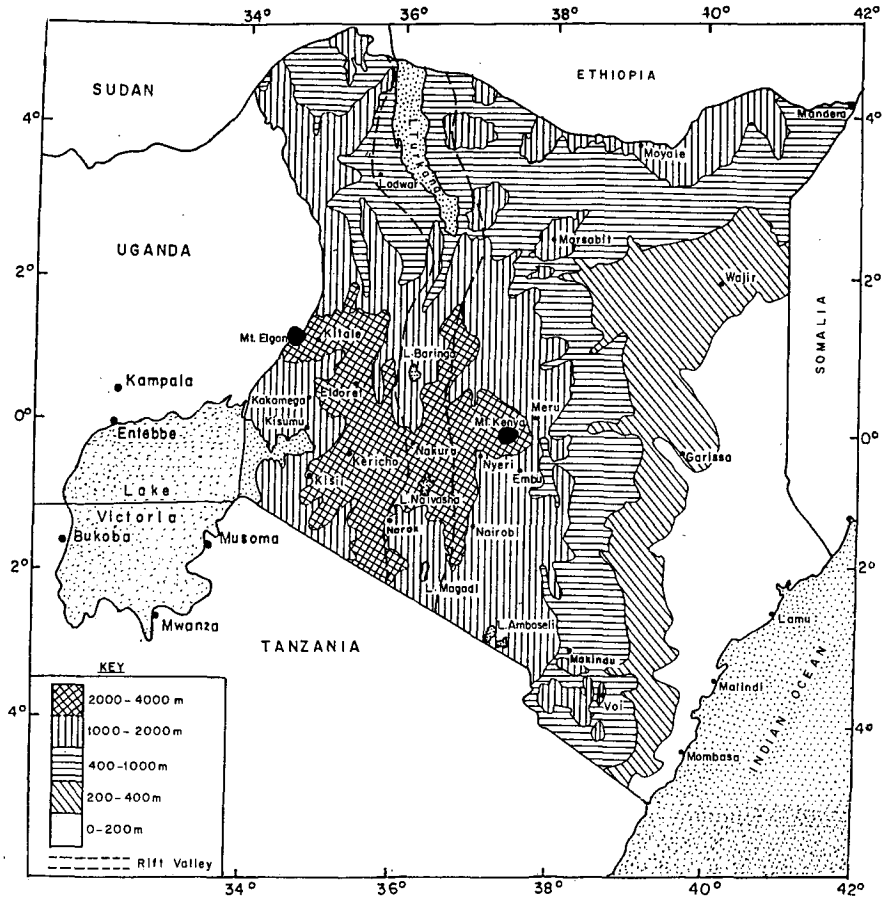

FIG. 1. The relief map of Kenya showing the synoptic stations used in the observational analysis, including the Lake Victoria region.

over the whole of Sudan and Ethiopia. At 100 mb (figure not shown) the winds were strongly easterly over Kenya attaining a maximum speed of 31.4 m s^{-1}. The winds at 100 mb emanated from an intense Mascarene anticyclone that had a significant equatorward displacement at this level.

The tephigram showing the radiosonde sounding over Nairobi (a city at 821-mb height, or about 1790 m above sea level, on the eastern slopes of the highlands) at 0000 UTC (figure not shown) depicted a calm wind condition at the surface with westerly winds in the layer from 700 to 400 mb and easterly winds in the upper troposphere. The relative humidity profile had a substantial amount of moisture in the atmospheric column (over 85% in the lower and middle troposphere). The tephigram showing the radiosonde ascent over Nairobi at 1200 UTC (Fig. 4) was characterized by the presence of easterlies at low levels (surface–650 mb), westerlies at midlevels (600–500 mb), and easterlies at the upper troposphere. The relative humidity profile showed the atmosphere to be quite humid from the surface to 500 mb with a value of 66% close to the surface and 84% in the intermediate layer above.

Figure 5 shows the 24-h rainfall (mm) that occurred over the country on 14 April 1985. The rainfall distribution was fairly widespread. The rainfall over the coastal region varied from 10 to 20 mm. Over the Kenya highlands and the Lake Victoria region the rainfall amount varied from 10 to 35 mm. The remaining areas of the country received between 5 and 10 mm of rainfall.

3. The numerical model used

a. General description

RAMS is a primitive equation prognostic model developed for the simulation and forecasting of weather systems and for depicting the results (Pielke et al. 1992). It has three major components:

- an atmospheric model that performs the simulations;
- an isentropic analysis package (ISAN) that prepares initial data for the atmospheric model from observed meteorological data (e.g., NMC, ECMWF, etc.);

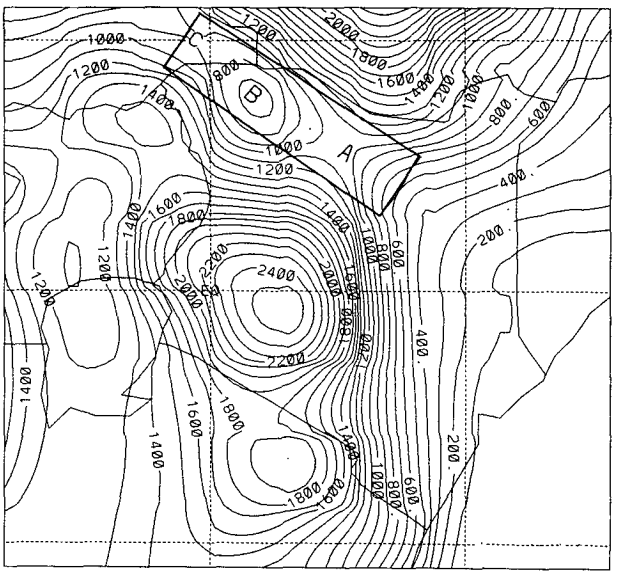

FIG. 2. Topography of the study area interpolated from a 10′ dataset. Contour interval is 100 m.

• a postprocessing model visualization analysis package (VAN) that interfaces the atmospheric model output with a variety of visualization software utilities.

A detailed description of RAMS, including the basic model equations, is given in Pielke et al. (1992). RAMS has many options, but only options pertaining to this study will be discussed briefly.

b. Domain and grid structure

Two grids were used in this study. The coarse grid domain was bounded by 14°N–14°S and 20°–50°E (Table 2). The fine grid domain was bounded by 6°N–6°S and 31°–44°E. Figure 1 shows the fine-grid model domain that covers the whole of Kenya and Lake Victoria, including portions of the surrounding countries. The horizontal fine-grid spacing was 20 km in both the east–west and north–south directions. There were 70 grid points in the x direction and 70 grid points in the y direction, with 30 sigma-z levels. The vertical grid spacing was 50 m near the ground with a geometric stretch ratio of 1–2 and a maximum stretch of 1500 m at the model top. The model top was at $\sigma_z = 20.6$ km (~50 mb). The geometric stretch ratio is used to provide a higher resolution close to the ground.

RAMS uses a two-way nesting procedure documented in Clark and Farley (1984). In this method, the different nested grids communicate with each other. The grid nesting thus allows a wider range of motion scales to be modeled simultaneously and interactively.

The grid structure uses the Arakawa C grid stagger (Messinger and Arakawa 1976). The advection operator is the flux form of the second-order leapfrog for the horizontal advection and a forward form of the vertical advection (Tremback et al. 1987). The time split scheme (Tremback and Kessler 1985) is used for the model time integration. The time step used for the fine grid was 45 s.

c. Cumulus parameterization

Cumulus parameterization is necessary to represent subgrid-scale transport by downdrafts and updrafts of cumulus clouds that vertically redistribute heat, moisture, and momentum within the model and also produce convective rainfall. A simplified version of the Kuo (1974) cumulus parameterization scheme as modified by Molinari (1985) was applied to compute convective precipitation rates (to help locate zones of deep convection) and accumulated cumulus convective precipitation. This scheme uses a one-dimensional cloud model to calculate the convective heating and moistening in a unit column of the atmosphere. There should be vertical motion at the cloud base to initiate convection. The threshold value of this vertical velocity at the diagnosed level of the cloud base in the model varies from -1 to 0.2 m s^{-1}. The more positive this parameter, the more difficult the initiation of convection. Convection will not occur if the cloud top is at a height

TABLE 1. Definitions of symbols used.

ITCZ	intertropical convergence zone
ECMWF	European Centre for Medium-Range Weather Forecasts
NMC	National Meteorological Center
UTC	universal time coordinated
CONTROL	control experiment (experiment 1)
MESO	mesoscale simulation (experiment 2)
SYNO	synoptic-scale monsoonal simulation (experiment 3)
SYNO.NLW	synoptic-scale monsoonal simulation with topography but without land–water contrast
SYNO.NTP	synoptic-scale monsoonal simulation with land–water contrast but without topography
MESO.NLW	mesoscale simulation with topography but without land–water contrast (orographic winds only)
MESO.NTP	mesoscale simulation with land–water contrast but without topography (sea–land-, lake–land-breeze only)
ACTUAL	averaged 24-h observed rainfall for 24 stations over Kenya on 14 April 1985
MSL	above mean sea level
ASL	above surface level; where "surface" refers to the terrain-following surface above sea level and ground level
EALLJ	east African low-level jet stream

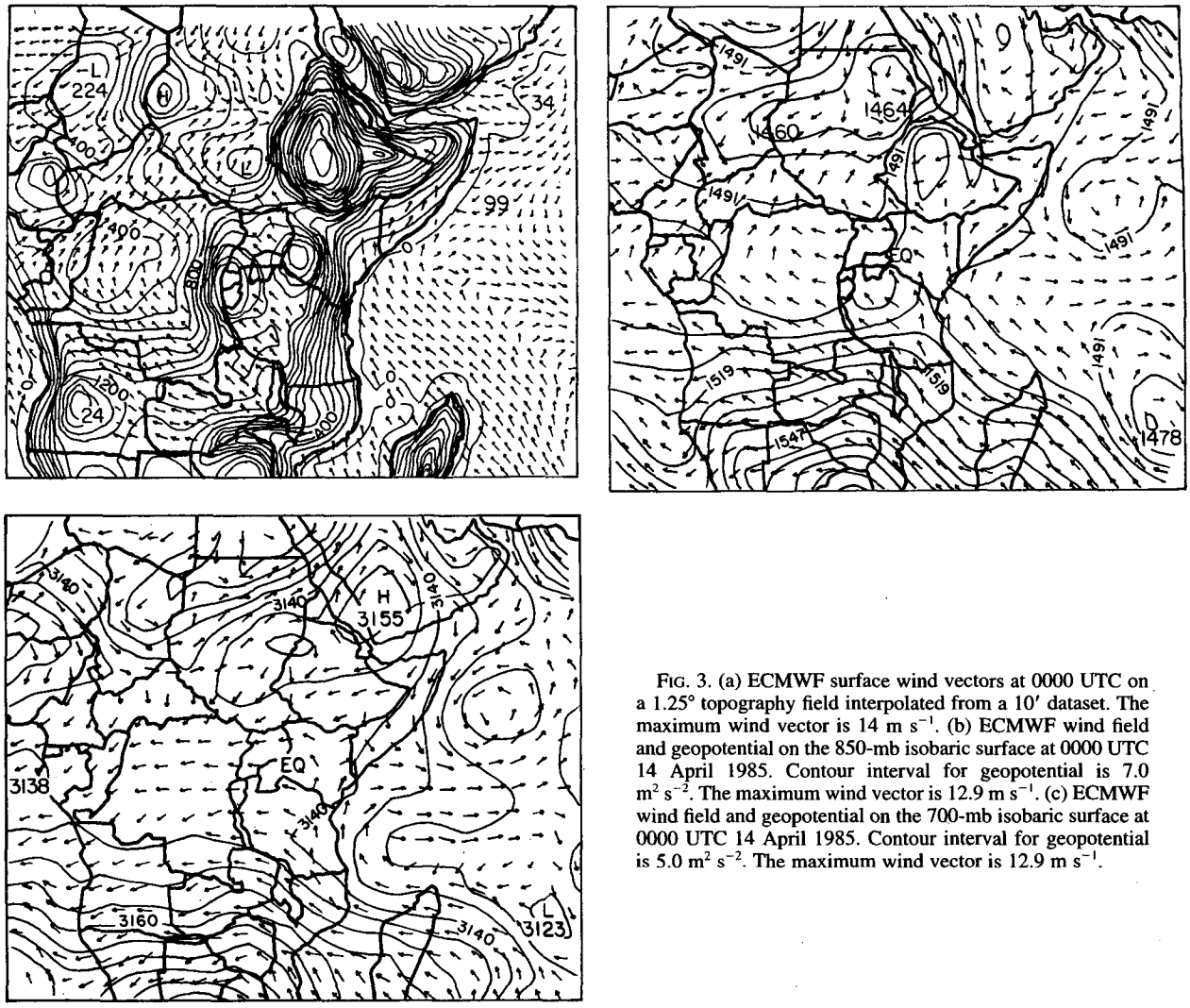

FIG. 3. (a) ECMWF surface wind vectors at 0000 UTC on a 1.25° topography field interpolated from a 10′ dataset. The maximum wind vector is 14 m s^{-1}. (b) ECMWF wind field and geopotential on the 850-mb isobaric surface at 0000 UTC 14 April 1985. Contour interval for geopotential is 7.0 m^2 s^{-2}. The maximum wind vector is 12.9 m s^{-1}. (c) ECMWF wind field and geopotential on the 700-mb isobaric surface at 0000 UTC 14 April 1985. Contour interval for geopotential is 5.0 m^2 s^{-2}. The maximum wind vector is 12.9 m s^{-1}.

below 500-mb level. A simplified downdraft–updraft scheme is similarly incorporated where the positive updraft area is weighted against the negative downdraft area. A fraction termed the "partition factor" (b) of the total moisture that converges into the unit atmospheric column is assumed to moisten the column whereas the remaining ($1 - b$) precipitates out.

d. Radiation parameterization

The radiation parameterization used was developed by Chen and Cotton (1983) and predicts the longwave and shortwave radiation tendencies. It includes the radiative effects of water vapor, ozone, and carbon dioxide.

e. Turbulent diffusion

RAMS, as applied in this study, uses a first-order eddy viscosity coefficient K that is a function of deformation and atmospheric stability given by a Richardson number enhancement (Tremback et al. 1987).

4. Initial and boundary conditions

a. Initial conditions

The daily gridded dataset from the global 2.5° × 2.5° ECMWF records, which have seven mandatory pressure levels along with the NMC rawinsonde and surface observation datasets, were used in this study to set the initial field and lateral boundary values for model integration for the CONTROL and SYNO experiments beginning at 0000 UTC. These datasets were accessed from the mass storage system runs at NCAR by a mesoscale isentropic data assimilation package (ISAN) for observed data developed by Tremback (1990). The seven mandatory pressure levels were 1000, 850, 700, 500, 300, 200, and 100 mb. The ECMWF pressure-level data access and analysis domain was bounded by the area 25°N–25°S and 5°–65°E. The number of grid

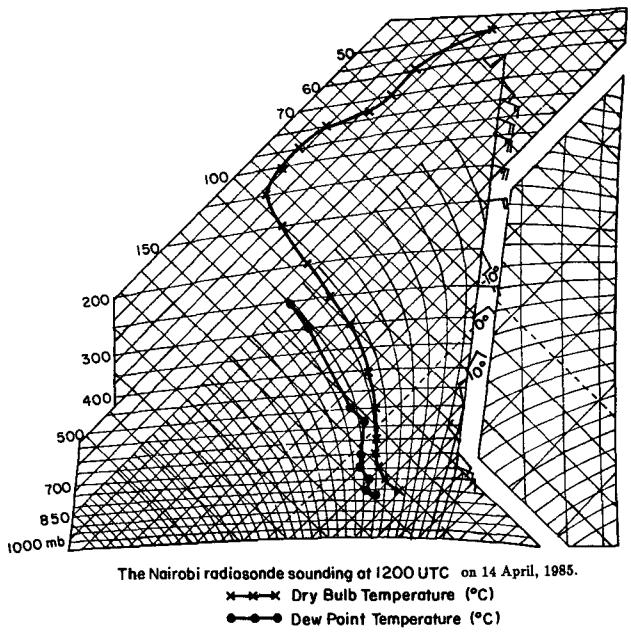

FIG. 4. The Nairobi radiosonde at 1200 UTC 14 April 1985.

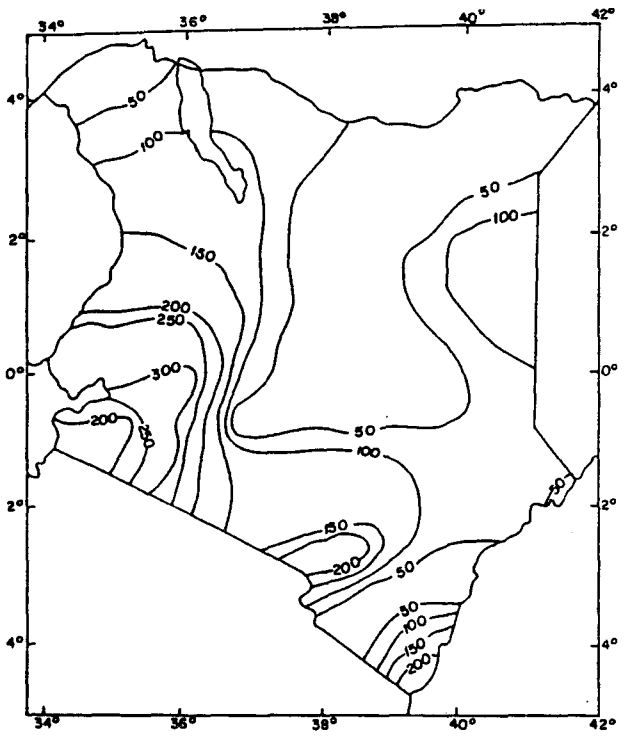

FIG. 5. Isohytes showing 24-h observed rainfall (mm) over Kenya on 14 April 1985.

points in the x direction was 25 with 21 grid points in the y direction.

In the ISAN package, during access of the pressure-level ECMWF (and NMC) gridded data, geostrophic adjustment is usually performed for the winds above the 100-mb level. In this study, however, it was found necessary to neglect the geostrophic adjustment at the upper level above 100 mb in the equatorial atmosphere after it was noted that inclusion of the geostrophic adjustment at the upper troposphere resulted in the generation of unique and well-defined cyclonelike vortices in the near-surface wind fields. These strong vortices in the equatorial latitudes were absent in the observed wind fields. The model was therefore left to extrapolate winds above the 100-mb level.

In order to be consistent with the exclusion of the geostrophic adjustment at the upper troposphere in the ISAN package during access of the ECMWF pressure-level analysis fields, Coriolis force was neglected in the atmospheric model for the equatorial atmosphere over Kenya. The neglect of the Coriolis force did not seem to drastically affect the wind flow pattern over the study domain.

The second stage considered the isentropic conversion of the ECMWF pressure-level data by vertical interpolation to isentropic levels over the same latitude–longitude bounds. The isentropic levels had intervals of 5 K from the surface to 360 K and intervals of 10 K from 370 to 400 K. This was to enable a finer resolution in the lower troposphere including the planetary boundary layer (PBL). The minimum θ at 1000 mb was 289.7 K and the maximum θ at 100 mb was 401.72 K. There were 19 isentropic levels generated between 1000 (or 289.7 K) and 100 mb (or 401.72 K). These levels were 290, 295, 300, 305, 310, 315, 320, 325, 330, 335, 340, 345, 350, 355, 360, 370, 380, 390, and

TABLE 2. Model options used.

	Experiment 1—CONTROL Experiment 2—MESO Experiment 3—SYNO
	Moist convection activated
• Grid system	3D simulation with coordinate transform activated
• Number of grids for run	2
• Model domain	
(i) Coarse-grid bounds	14°S–14°N, 20°–50°E
Horizontal grid spacing	Δx = 80 km; Δy = 80 km
Time step	Δt = 90 s
Vertical grid spacing	50 m
Vertical stretch ratio	1:2
Maximum Δz for vertical grid stretch at the model top:	1500 m
Number of grid points	x: 42; y: 42; z: 30
(ii) Fine-grid bounds	6°S–6°N, 31°–44°E
Horizontal grid spacing	Δx = 20 km; Δy = 20 km
Time step	Δt = 45 s
Vertical grid spacing	50 m
Number of grid points	x: 70; y: 70; z: 30

400 K. The rawinsonde reports were objectively analyzed to the isentropic grid by the Barnes scheme (1973). Similarly, surface observation data were objectively analyzed to the horizontal grid using the Barnes scheme (1973). The surface observations and the rawinsonde datasets were used to enhance the ECMWF pressure-level data during the vertical interpolation of the data to isentropic levels.

A 10′ (0.16666°) global-averaged terrain height dataset was used for this study. The analysis domain for topography was bounded by 30°N–30°S and 0°–70°E. The number of grid points in the x direction (longitude) was 421, with 361 grid points in the y direction. Similarly, a global 1.0° × 1.0° sea surface temperature dataset was accessed from the mass storage system at NCAR. The number of grid points were 360 in the x direction and 181 in the y direction.

The Barnes (1973) objective analysis scheme was again applied to smooth out analyzed results by removing the two grid increment ($2\Delta s$) waves that are known to generate meteorological "noise" in the model output (Pielke 1984).

The mesoscale experiment (MESO) used one-station sounding data from Dagoretti Weather Station in Nairobi. A horizontally homogeneous initialization technique was performed using RAMS to create the initial fields at 0000 UTC.

b. Boundary conditions

The lower boundary conditions used the surface layer and soil model parameterizations developed by Tremback and Kessler (1985). The model calculates a surface budget that includes shortwave and longwave fluxes and conduction to and from the soil. The "wall on top" was used as a top boundary condition. The lateral boundary condition used the Davies (1976) relaxation method to nudge the RAMS solution to the observations. The nudging is weighted at the five outermost points. The model was run using a nonhydrostatic option.

c. Map projection used

Although polar stereographic coordinates are suitable for higher latitudes and Mercator coordinates give less distortion at low latitudes (40°N–40°S), the former can be applied over any specified region of the globe by simply placing the tangent plane of projection at the center of the domain of interest (Tremback 1990, personal communication). A polar stereographic projection is a mapping between the spherical earth and a Cartesian plane tangent to the earth, with all projection lines emanating from the point on the earth's surface opposite or antipodal to the point of tangency. The Cartesian model plane is centered around the point of tangency, which may be placed anywhere on the earth (the pole in this case refers to the point of tangency specified at the center of the domain, not to either geographic pole). Thus, distortion in the center of the domain is zero between the spherical earth and the model grid. The distortion increases outward (gradually) toward the model lateral boundaries. This transformation allows the model to cover geographic domains up to hemispheric in size and avoids the numerical problems encountered near the geographic poles when latitude–longitude coordinates are used. In this study the point of tangency at the center of the model domain was at 0° latitude and 35°E.

5. Numerical simulations

A series of three simulations were performed to reproduce the wind flow pattern and weather that prevailed over Kenya on 14 April 1985. Each simulation was integrated forward in time to 24 h beginning at 0000 UTC or 0300 local time. Tables 2 and 3 summarize the model options and initial characteristics used in the simulations.

1) The first control experiment (CONTROL) used full physics and moist convection in simulating the large-scale flow fields over the country using the ECMWF data of 0000 UTC 14 April 1985 to initialize the model. The modeled results were compared to some ECMWF analysis fields at 1200 UTC and to the available observations (surface winds and rainfall) in order to determine the ability of RAMS in replicating the known synoptic-scale features in Kenya.

2) The simulation in the second experiment (MESO) was started from an atmosphere at rest ($u = 0$, $v = 0$, $w = 0$) and excluded the synoptic-scale monsoonal flow from the model runs. This experiment simulated the dynamical, thermodynamic, and moisture structure of the atmosphere in Kenya in the absence of the large-scale monsoonal flow. Moist convection was also included in the model simulation.

3) The third experiment (SYNO) was run without terrain ($x = 0$) and land–water contrast in order to eliminate the effect of the thermally induced local forcings and to clearly isolate and identify the large-scale monsoonal flow and its influence on the weather in Kenya. Terrain was thus, in our study, considered a local feature that generates upslope and downslope drainage winds and also modifies the large-scale temperature, moisture, and wind flow patterns over the country. Similarly, the land–water contrast, which is brought about by the presence of the large water bodies (like Lake Victoria, Lake Turkana, and the Indian Ocean), was considered responsible for the generation of strong sea–land- and lake–land-breeze circulations and had to be excluded.

The total grid-averaged convective rainfall amounts generated over Kenya in the MESO and SYNO experiments were compared with that in the CONTROL experiment in order to identify the contribution of the large-scale monsoonal winds and the mesoscale systems on the convective rainfall over the country.

TABLE 3. Initial model characteristics.

	Experiment 1—CONTROL	Experiment 2—MESO	Experiment 3—SYNO
Initial field for the two grids	Variable initialization at 0000 UTC	Horizontally homogeneous initialization 0000 UTC	Variable initialization 0000 UTC
Pressure calculation	Nonhydrostatic	Nonhydrostatic	Nonhydrostatic
Vertical velocity diagnosis	Incompressible	Incompressible	Incompressible
Top boundary condition	"Wall on top"	"Wall on top" Rayleigh friction layer with five top points	"Wall on top"
Lateral boundary conditions	Davies (1976)	Klemp–Wilhelmson (1978) with phase speed = 20 m s^{-1}	Davies (1976)
Finite differencing	Second-order horizontal, second-order vertical	Second-order horizontal, second-order vertical	Second-order horizontal, second-order vertical
Cloud option	Level 3—microphysics activated	Level 3—microphysics activated	Level 3—microphysics activated
Radiation parameterization	Chen and Cotton (1983)	Chen and Cotton (1983)	Chen and Cotton (1983)
Soil moisture parameterization	Tremback and Kessler (1985)	Tremback and Kessler (1985)	Tremback and Kessler (1985)
Cumulus parameterization	Modified Kuo (1974)	Modified Kuo (1974)	Modified Kuo (1974)
Threshold value for vertical velocity at cloud base	0.01 m s^{-1}	0.01 m s^{-1}	0.01 m s^{-1}

6. Results and discussion

a. The large-scale wind and pressure fields in the CONTROL experiment

The lowest-level modeled monsoonal winds for the CONTROL experiment at 0600 UTC (0900 LT) are shown in Fig. 6a. The monsoonal wind current entered Kenya in a southwesterly direction at the coast and a southeastern portion of the country and over the Indian Ocean. However, part of the monsoonal current bifurcated to an almost southeasterly–easterly trajectory to the western and northwestern part of the country. This westward flow of the monsoonal current, which spills over the almost meridionally oriented high elevation terrain (see Figs. 1 and 2), is attributed to the presence of an orographically-induced trough over western Kenya, Uganda, Sudan, and central Africa (Semazzi 1980). The mean observed surface winds for the month of April 1985 at 0600 UTC are depicted in Fig. 6b. Figure 7a shows the lowest-level modeled monsoonal winds 6 h later at 1200 UTC (1500 LT). The flow pattern showed a strong topographic influence as the winds converged at the highest point in the model domain over the western part of the country. The mean observed surface winds for 1200 UTC April 1985 are displayed in Fig. 7b. The model-predicted winds in Fig. 6a at 0600 UTC and in Fig. 7a at 1200 UTC at 23.9 m above surface level (ASL) are in good agreement over much of the country, with the mean observed surface winds (10-m anemometer height) in Figs. 6b and 7b, respectively, allowing for the surface frictional effects due to the slight difference in the heights of the two levels and smoothing of the topography used in the simulation.

The justification for comparing the model-predicted surface wind fields (Figs. 6a and 7a) with the near-surface mean winds for the month of April (Figs. 6b and 7b) can be explained as follows.

In the Tropics, the wet and dry periods (or seasons) are a bit constant or the large-scale systems are quasi-stationary (Asnani 1993). This means that the large-scale systems like the ITCZ or the NE and SE monsoonal wind currents do not change radically from one day to another but persist for months in a region. This generally implies that monthly mean synoptic-scale winds will resemble the synoptic-scale winds for any day within the month. The deviations are due to perturbations that are superimposed on the basic monsoonal currents. As stated in section 1 of this text, one of the criteria used for choosing the data for the case study (14 April 1985) was that this particular day displayed synoptic conditions reminiscent of an average April weather situation (the other criteria was the presence of a fairly widespread rainfall over the country). Therefore, to verify the validity of the above-stated criterion, comparison was made between the model-predicted winds at 23.9 m ASL and the mean surface wind for April 1985.

The axis of the intertropical convergence zone (ITCZ) was not detectable in the wind field at the lowest levels of the model but is clearly evident at 2.68 km ASL (≈726 mb) as a zone of wind discontinuity and convergence between the two hemispheric monsoonal air currents, the NE and the SE winds (Fig. 8a). The ECMWF analysis field at 1200 UTC (Fig. 8b) shows the convergence of the two hemispheric air currents (SE and NE) at the 700-mb level. The diffuse nature of the ITCZ at the surface and at the 850-mb isobaric level in east Africa and its manifestation between 750 and 700 mb is documented in Kiangi et al. (1981), among others.

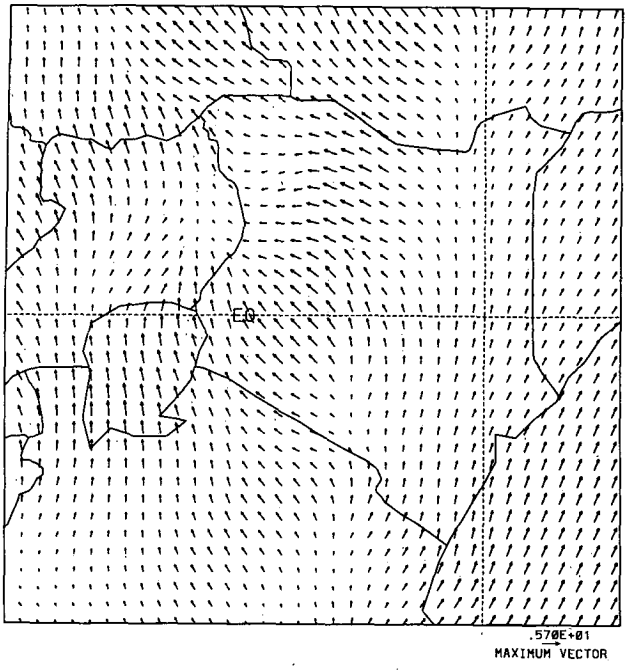

FIG. 6. (a) Model-predicted wind vectors at 23.9 m ASL at 0600 UTC (CONTROL). (b) Observed mean surface streamline isotach analysis for April 1985 at 0600 UTC.

Figure 9a depicts the model-predicted winds in the midtroposphere over Kenya at 5.73 km (~500 mb) after 12 h of simulation. The winds are northerly to northwesterly over the eastern half of the country and over the Indian Ocean. The remaining western half of the country has a northerly to northeasterly wind current. Generally, the simulated winds over Kenya have

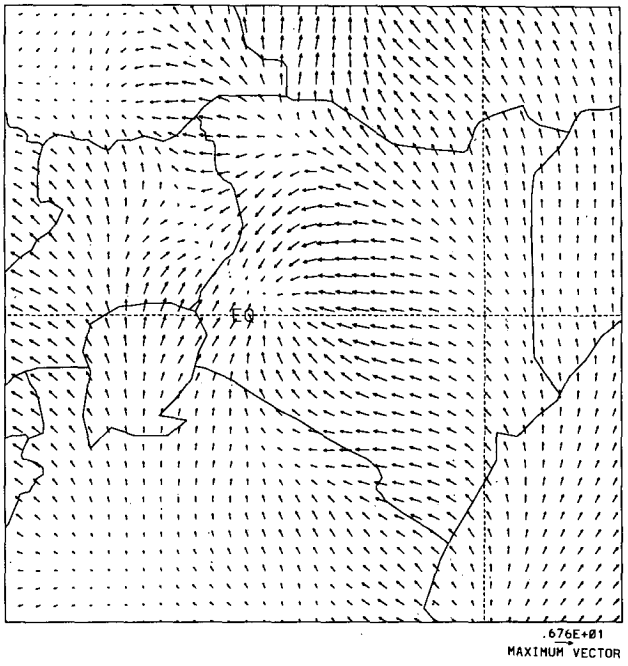

FIG. 7. (a) Model-predicted wind vectors at 23.9 m ASL at 1200 UTC (CONTROL). (b) Observed mean monthly surface streamline isotach analysis for April 1985 at 1200 UTC.

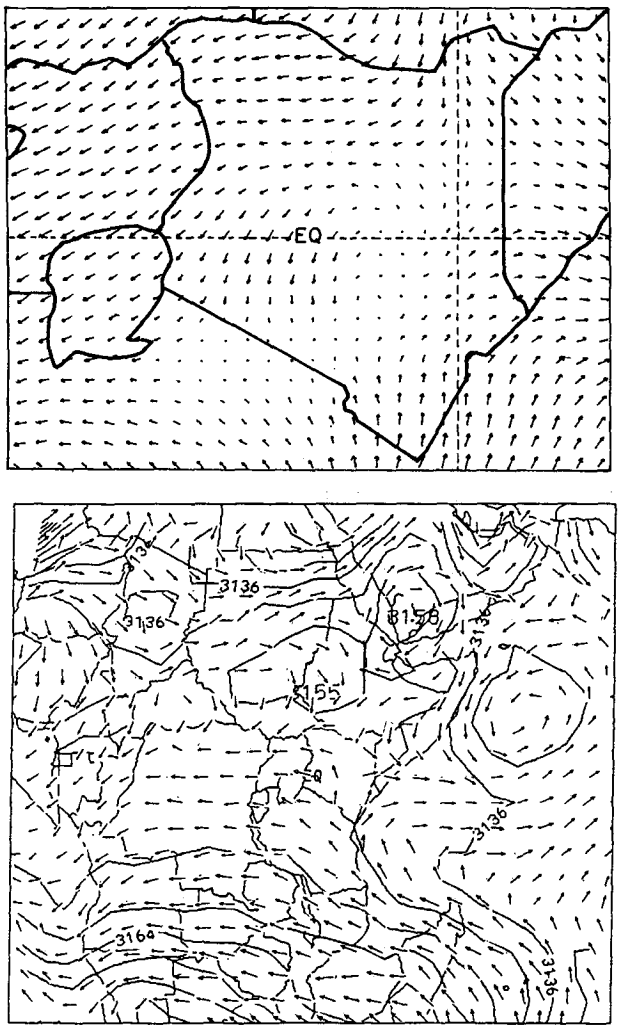

FIG. 8. (a) Simulated wind vectors at 2.681 km ASL at 1200 UTC showing zones of wind discontinuity and convergence between the NE and SE monsoonal currents. (b) ECMWF wind vectors on the 700-mb isobaric surface at 1200 UTC. Contour interval is 5.0 $m^2 s^{-2}$. The maximum wind vector is 20 m s^{-1}.

a strong northerly meridional component. The winds attain a maximum speed of 7.9 m s^{-1} at this level.

Figure 9b shows the 500-mb ECMWF analyzed wind field at 1200 UTC. Comparison of Fig. 9a to Fig. 9b shows that there is good agreement between the model-predicted winds and the observed winds in the midtroposphere over the country.

The wind field predicted by the model over Kenya in the upper troposphere at 16.9 km (~100 mb) after 12 h of simulation is shown in Fig. 10a. The upper-level easterlies are strongly zonal over the country, with a maximum speed of 13.5 m s^{-1}. The ECMWF analyzed wind field at the 400-K isentropic surface (~100 mb) is displayed in Fig. 10b and depicts an easterly current that is strongly zonal over Kenya. Comparison of Fig. 10a to Fig. 10b helps to illustrate the close agreement between the predicted and the observed winds at the upper troposphere over Kenya.

The east African low-level jet stream (EALLJ) at the coast was revealed in the simulation as a wind speed maximum in the low-level flow at 1.4 km MSL (Figs. 11a and 11b). The wind maximum (area marked C in Fig. 11b) moved northward and inland over the Garissa area, decreasing in speed from 17.0 m s^{-1} at 0000 UTC (figure not shown) to 12.8 m s^{-1} at 1200 UTC (Fig. 11b). The decrease in speed was attributed to the vertical transfer of momentum through vertical mixing generated in the boundary layer. This jet stream is known to be steady in direction but variable in speed and attains maximum intensity in July/August at about 1.5 km MSL at the coast (Findlater 1972; Bannon 1979).

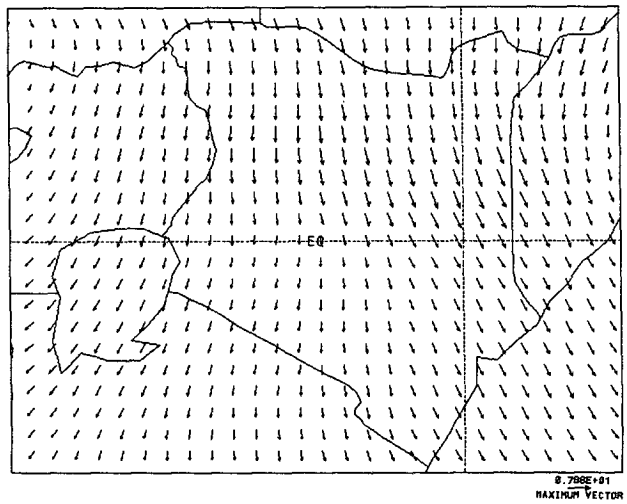

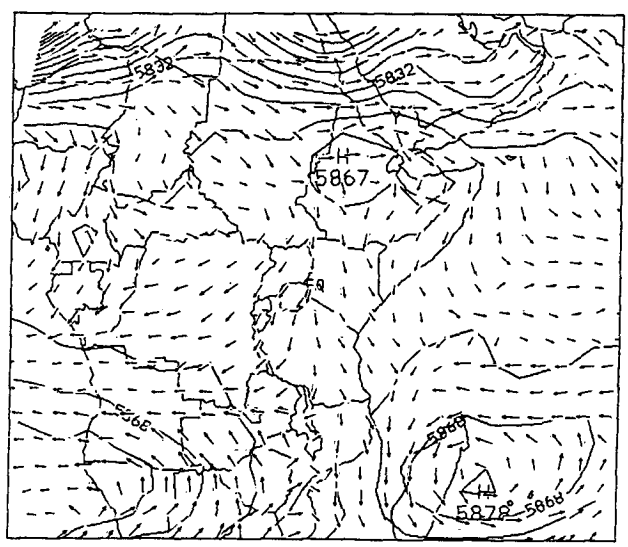

FIG. 9. (a) Simulated wind vectors at 5.73 km ASL (~500 mb) at 1200 UTC (CONTROL). (b) ECMWF wind vectors on the 500-mb isobaric surface at 1200 UTC 14 April 1985. Contour interval is 6.0 $m^2 s^{-2}$. The maximum wind vector is 31.5 m s^{-1}.

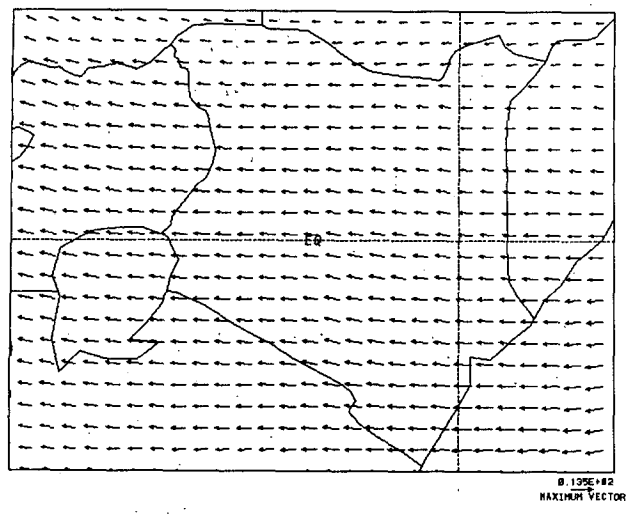

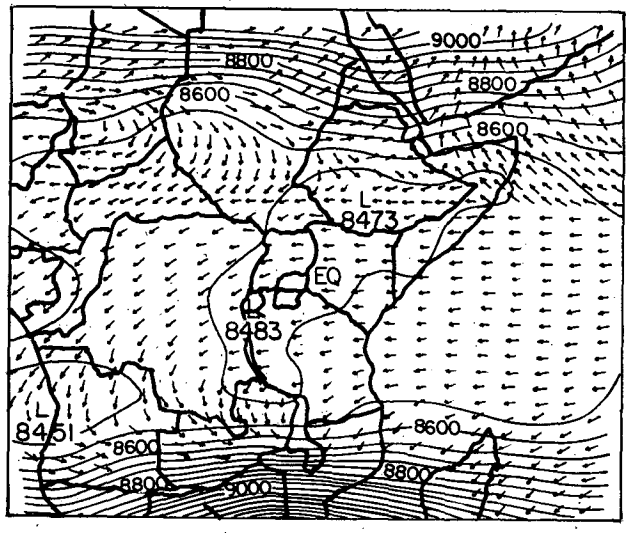

FIG. 10. (a) Simulated wind vectors at 16.9 km (~100 mb) at 1200 UTC (CONTROL). (b) ECMWF wind vectors on the 400-K isentropic surface (~100 mb) at 1200 UTC 14 April 1985. The maximum wind vector is 18.0 m s^{-1}. The pressure contour interval is 0.05 kPa.

The vertical velocity field at the lowest model level (23.9 m ASL) showed an interesting pattern around Lake Victoria, an inland freshwater body that lies in a depression between the east African highlands to the east and the central African highlands to the west (see Fig. 2).

The modeled vertical wind field at 1.16 km ASL predicted (above the planetary boundary layer, PBL) in the morning at 0500 UTC (0800 lt) in Fig. 12a showed rising motion (solid lines) over much of Lake Victoria, the western region of the lake, the Turkana–Marsabit corridor, the coastal region, and other low lands. This motion was indicative of horizontal velocity convergence over these low-elevation areas. The rising motion on the western part of the lake was attributed to convergence associated with the upslope component of the large-scale monsoonal current as it rises over the higher grounds in central Africa. This monsoonal current is decelerated at low levels by the combined downslope drainage winds and the land-breeze circulation flowing in the opposite direction toward the lake. There was strong horizontal subsidence motion (dotted lines) to the eastern part of the lake including the highland areas. The subsidence motion over the eastern part of the lake was linked to the downslope flow pouring into the Lake depression from the Kenya highlands. The flow is composed of the large-scale monsoonal current, with a downslope component that is accelerated at lower levels by the katabatic winds from the higher grounds combined with the land breeze flowing toward the lake. The subsidence motions over the higher lands at 0500 UTC was attributed to radiative cooling.

The simulated vertical velocity field at 1200 UTC (Fig. 12b) showed this stronger rising motion over the high grounds as compared to the low-elevation areas.

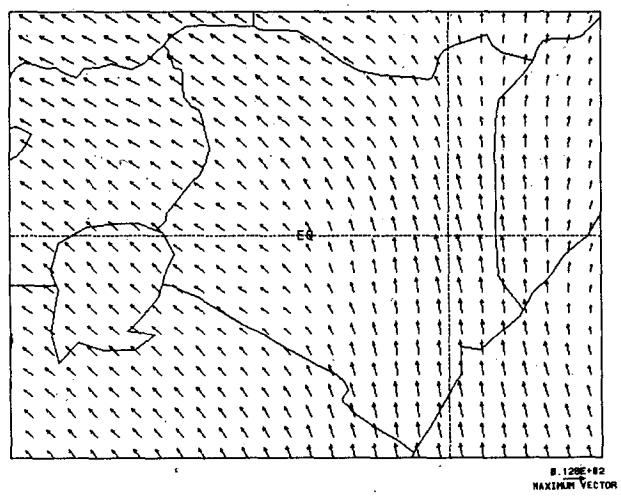

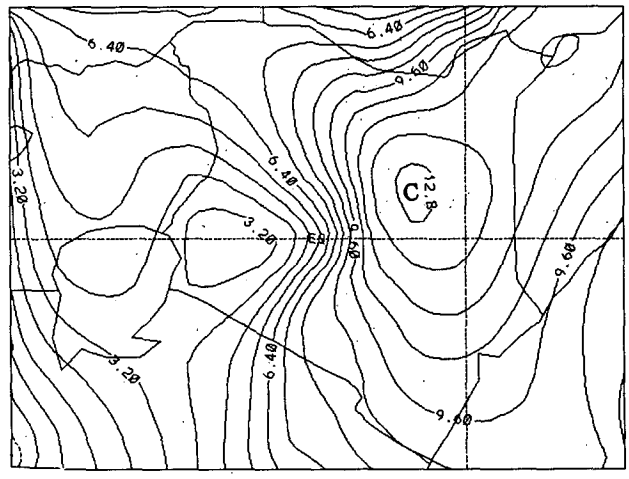

FIG. 11. (a) Simulated wind vectors at the level of the EALLJ (1.4 km ASL) at 1200 UTC. (b) Simulated contour isotachs showing wind speeds at the level of the EALLJ (1.4 km ASL) at 1200 UTC. The contours vary from −0.6 to 12.8 m s^{-1}. The contour interval is 0.8 m s^{-1} (CONTROL).

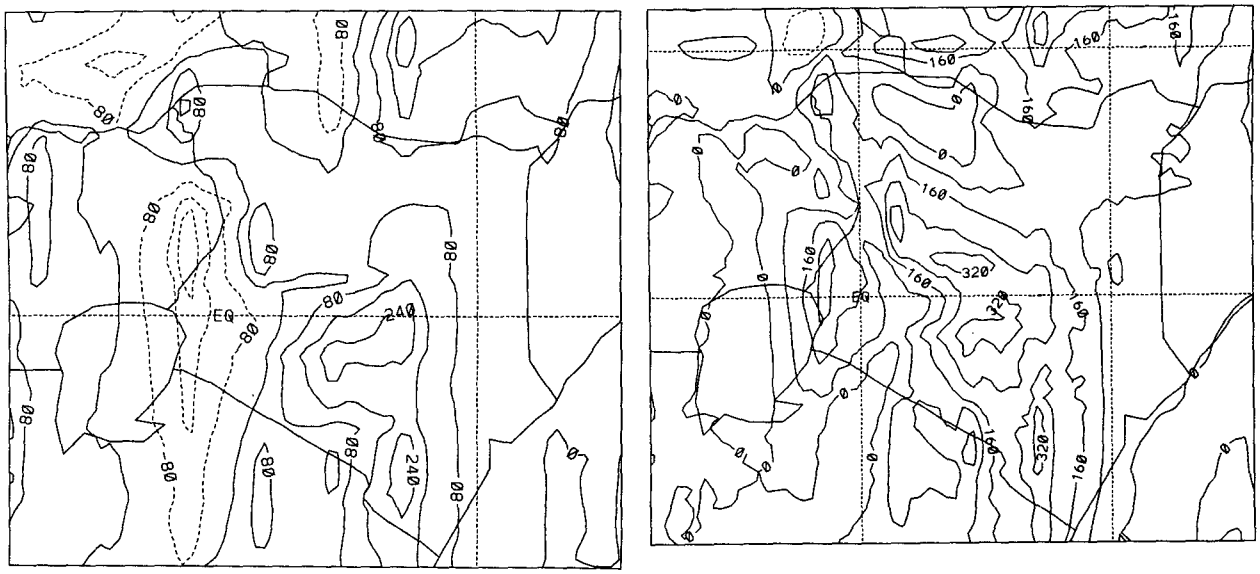

FIG. 12. (a) The simulated vertical wind field w at 1.16 km ASL at 0500 UTC showing contours from -1.6×10^{-2} to 1.6×10^{-2} m s^{-1}. Contour interval is 0.008 m s^{-1} (CONTROL). (b) The simulated vertical wind field w at 1.16 km ASL at 1200 UTC showing contours from -8.0×10^{-2} to 4.0×10^{-2} m s^{-1}. Contour interval is 0.008 m s^{-1} (CONTROL).

Stronger vertical velocities were registered over the eastern slopes of the Kenya highlands as compared to the western slopes. There was little vertical motion over the Turkana–Marsabit corridor, along the coast, and over the Lake Victoria depression–except to the northeastern part of the lake.

Distinct pressure relative minimum and maximum regions at 144 m ASL, apparently induced by the general flow pattern and the ITCZ, were simulated over the country; one to the west (local high, H) and the other to the east (local low, L) as depicted in Fig. 13. A low pressure cell that intensified more than the one over Kenya during the afternoon was simulated over central Uganda, spreading over Lake Victoria and the western part of Kenya. This low pressure cell was oriented in a northwest–southeast direction over Uganda with almost a meridional alignment over the lake. The low pressure regions over the study domain may define the ITCZ position at lower levels, which is usually diffuse or absent in synoptic charts owing to interference by the complex terrain over the study area. The low pressure cell over Uganda that extended over Lake Victoria may be linked to the Lake Victoria trough, which is induced by the orographic flow of the monsoonal current over the somewhat meridionally oriented East African highlands (Semazzi 1980).

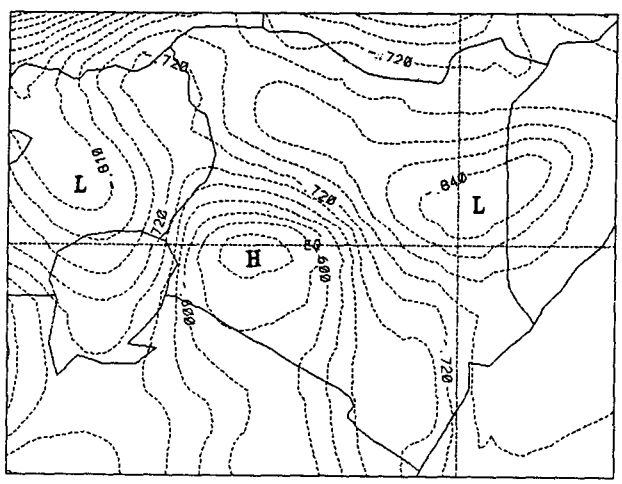

FIG. 13. Perturbation Exner function at 144 m ASL at 1200 UTC. Contour values are in joules per kelvin per kilogram (CONTROL).

b. The large-scale temperature and moisture in the CONTROL experiment

The diurnal evolution of the thermodynamic structure over the study domain is documented by the near-surface potential temperature θ_s at 0000 UTC and at 1200 UTC illustrated in Figs. 14a and 14b, respectively. For instance, the value of θ_s registered over much of Lake Victoria at 0000 UTC was 302 K. At 1200 UTC the temperature over much of the lake increased to a value of about 307.5 K. This was an increment of about 5.5 K in temperature during the first 12 h of simulation. More rise in temperature was recorded over the lowlands than at the higher elevations. A slight increase in the large-scale temperature (or moisture) field in the Tropics can have a profound effect on the weather since humidity is high (Asnani 1993).

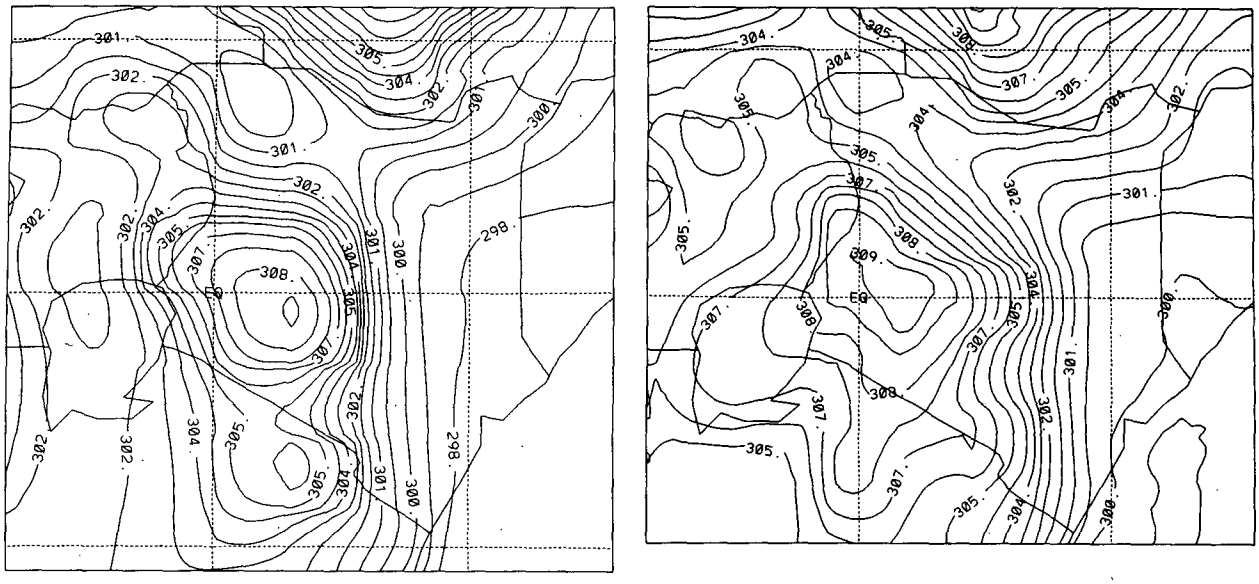

FIG. 14. (a) The simulated potential temperature field at 23.9 m ASL at 0000 UTC showing contours from 297.5 to 308.7 K. Contour interval is 0.7 K (CONTROL). (b) The simulated potential temperature field at 23.9 m ASL at 1200 UTC showing contours from 298.2 to 310 K. Contour interval is 0.7 K (CONTROL).

The horizontal structure of the large-scale potential temperature in the lower and midlevels of the atmosphere depicted contour patterns that were closely aligned to the complicated topography over the country. The orientation of the isentropes depicted the presence of a "cold pool" of air simulated in the Turkana–Marsabit corridor (Figs. 14a and 14b). The "cold pool" was indicative of a cold surge of air incursion into central Africa from the Indian Ocean infiltrating through this gap that lies between the Ethiopian highlands to the north and the Kenyan highlands to the south (Fig. 2). The "cold pool" was more intense at 1200 UTC than at 0000 UTC since the curvature of the isentropes are sharper during the afternoon.

The large-scale moisture field (figure not shown) at the lowest model level (23.9 m ASL) depicted a maximum of 18.4 g kg^{-1} at 0500 UTC (0800 LT) along the northern coast adjacent to the Indian Ocean with decreasing values inland. This maximum increased to 20 g kg^{-1} during the afternoon, which advected and spread inland to the north and west over the low pressure areas, thereby demonstrating the effect of the large-scale monsoonal wind on the transfer of moisture inland from the Indian Ocean.

c. *Precipitation pattern for the CONTROL experiment*

The modeled convective precipitation rates given by rainfall maps at different times of simulation (figures not shown) showed zones of deep convection in areas where the vertical motion occurred as discussed above. During late night and early morning, convective precipitation occurred over the western region of Lake Victoria, over the coastal area including the adjacent lowlands, and over the Turkana–Marsabit corridor. These areas experienced rising motion during the early hours of model integration (Fig. 12a). Some of this deep modeled convection showed a westward advection by the large-scale monsoonal winds during the daytime hours. During the afternoon hours, the convective precipitation rain was conspicuously absent over the western region of Lake Victoria, over the Turkana–Marsabit corridor, and along the coastal strip. These areas did not experience rising motion during the day as was shown previously (Fig. 12b). During the afternoon period, convective precipitation occurred mostly over the high-elevation areas including the eastern part of Lake Victoria. The 24-h accumulated convective precipitation predicted by the model is shown in Fig. 15 (at a contour interval of 2.5 mm). Compared to the 24-h observed rainfall over the country in Fig. 5, the predicted convective rainfall was less in magnitude than the observed precipitation, especially over the highlands and eastern part of Lake Victoria. The model predicts four regions of maximum rainfall. The maximum in northwestern Kenya (area marked A in Fig. 15) does not correspond to any maximum over the same area in the observed field (Fig. 5). The somewhat S-shaped elongated maximum predicted in central Kenya (area marked B in Fig. 15) is not well reflected in the observations (Fig. 5). The predicted narrow maximum running in the north–south direction along the southwest Kenya border (area marked C in Fig. 15) does not look like the much larger, broad maximum extending northeastward in the observations (Fig. 5). Finally, the maximum in the predicted field in southeastern Kenya (area marked D in Fig. 15) is located

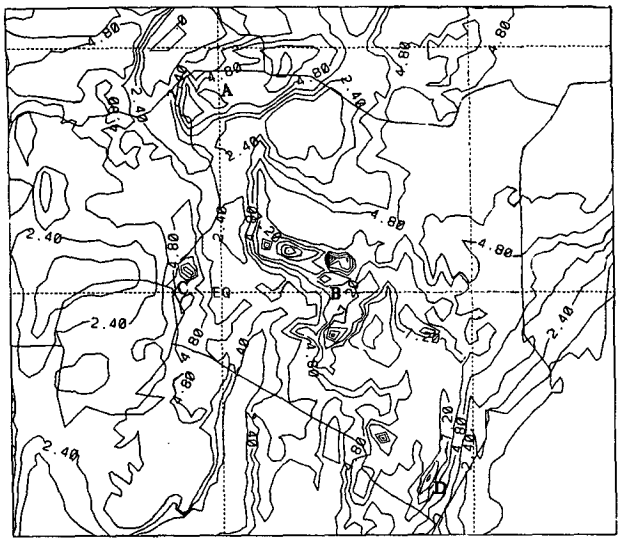

FIG. 15. The 24-h accumulated precipitation (mm) from convective parameterization on 14 April 1985. Contour interval is 2.5 mm (CONTROL).

distinctly inland whereas the observations show a maximum right on the southeast coast.

This discrepancy in the spatial distribution of the model predicted convective rainfall amounts and the observed rainfall may be attributed in part to the representation of topography in the model and to the spatial resolution. Figures 1 and 2 will show that the 10′ topography used in the model is very much smoothed, especially over the high-elevation areas that fall between 2000 m MSL and above. It is envisaged that a 5′ topography would better represent the complex inhomogeneous terrain features over Kenya. Finer spatial resolution (e.g., 15 or 10 km) would resolve convective rainfall better (Bougeault 1992). The 24-h grid-averaged value computed from the output of the predicted accumulated convective rainfall at every grid point over Kenya was 9.4 mm.

Figures 16a and 16b show the time series (hour by hour) of the convective precipitation (mm h^{-1}) averaged over all stations in which rainfall data was available (see Fig. 1). Figure 18c shows the histogram for the 24-h grid-averaged values computed from the output of the predicted 24-h accumulated convective rainfall at every grid point over Kenya for various experiments performed (several of which are discussed in the next section of this paper). To obtain the estimate of the observed areal rainfall, individual 24-h autographic records from 24 stations over Kenya with automatic rain gauges (Fig. 1) were used to obtain hourly averaged rainfall for all the stations and 24-h averaged total precipitation for all the 24 stations over the country on 14 April 1985. These records are depicted as actual observed hourly averaged time series of precipitation (ACTUAL) in Fig. 16a and as a histogram of actual observed 24-h averaged total precipitation over the country in Fig. 16c. While the observed data are not uniform across Kenya, they constitute the only data available in which to validate the realism of the model. In Fig. 16a, both the peaks of the CONTROL and the ACTUAL occur 2 h apart at 1600 and 1800 LT, respectively. This time lag in the peak rainfall may be attributed to the smoothed topography used in the model and the need for a finer spatial resolution. However, the 24-h grid-averaged convective precipitation value over Kenya for the CONTROL of 9.4 mm was below the ACTUAL rainfall value of 16.5 mm.

A dense and uniform observational network of automatic rain gauges over the country would have given a value of areal rainfall distinctly different from the one computed from the 24 synoptic stations (i.e., 16.5 mm). This is because rainfall is the meteorological element with the highest spatial variability in Kenya and the rest of east Africa than either temperature or pressure (Beltrando 1990; Asnani 1993). This means that the value of the rainfall amount can change drastically from one station to another located a few kilometers away. For instance, Voi recorded 1.9 mm on 14 April 1985, whereas Makindu (a close station) had 22.0 mm of rainfall. Similarly, Mombasa had 19.5 mm of rainfall, whereas Malindi (Fig. 1) recorded only 1.2 mm.

Two experiments were performed in order to isolate the effects of the synoptic-scale and mesoscale forcings on the rainfall that occurred over Kenya on 14 April 1985.

d. Isolating the impact of the mesoscale circulation on the rainfall over Kenya (MESO experiment)

In this experiment (MESO), the simulation was started from an atmosphere at rest ($u = 0$, $v = 0$, $w = 0$) in order to generate the terrain-induced mesoscale circulations that are caused by differential thermal heating resulting from the topographic inhomogeneity and the land–water contrast. The precipitation processes were included in the simulation.

The mesoscale wind streamlines at 23.9 m ASL during the early morning at 0500 UTC (0800 LT) displayed in Fig. 17a show katabatic drainage winds flowing downslope from the highlands toward the low-elevation areas. There is horizontal velocity convergence over Lake Victoria, the Indian Ocean, and the Turkana–Marsabit corridor and low-level velocity divergence over the highlands as is depicted in the wind streamlines. The low-level horizontal velocity convergence over Lake Victoria, the Indian Ocean, and other low-elevation areas resulted in rising motion and subsequent convective precipitation over these areas. The convergence over Lake Victoria is a consequence of the resultant nonlinear interaction between two mesoscale circulations: the land–lake breeze and the katabatic downslope drainage winds, both of which flow toward the lake during the early morning period.

During the afternoon, the wind streamlines reversed in direction as shown in Fig. 16b at 1200 UTC (1500

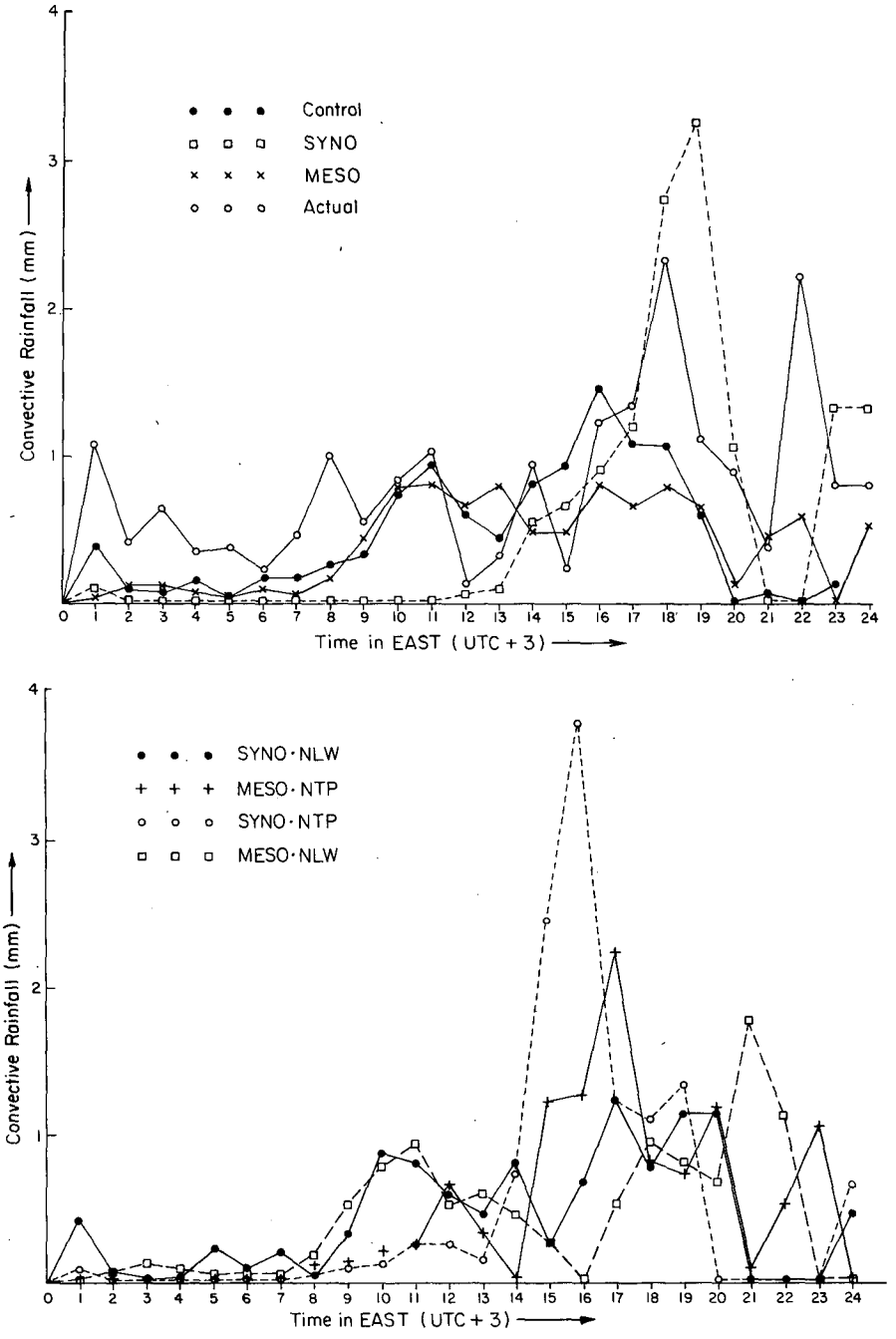

FIG. 16. (a) Time series of convective precipitation for different simulations and the actual observed average rainfall over Kenya on 14 April 1985. (b) Time series of convective precipitation for various sensitivity experiments over Kenya on 14 April 1985. (c) Histogram showing grid-averaged 24-h convective precipitation for different experiments and the actual observed average rainfall over Kenya on 14 April 1985.

LT). There was low-level horizontal velocity divergence over Lake Victoria, the Indian Ocean, the Turkana–Marsabit corridor, and other low-elevation areas. The strong sea breeze at the coast coupled with the anabatic upslope winds to converge over the highlands. This coupling of the sea breeze and the anabatic winds (mesoscale-to-mesoscale interaction) advects the sea-breeze impact (heat, moisture, and momentum) far inland. The vertical wind field (figure not shown) showed stronger rising motion over the high grounds (with a maximum value of 4.0 cm s^{-1}) as compared to the lowlands. The rising motion caused by the low-

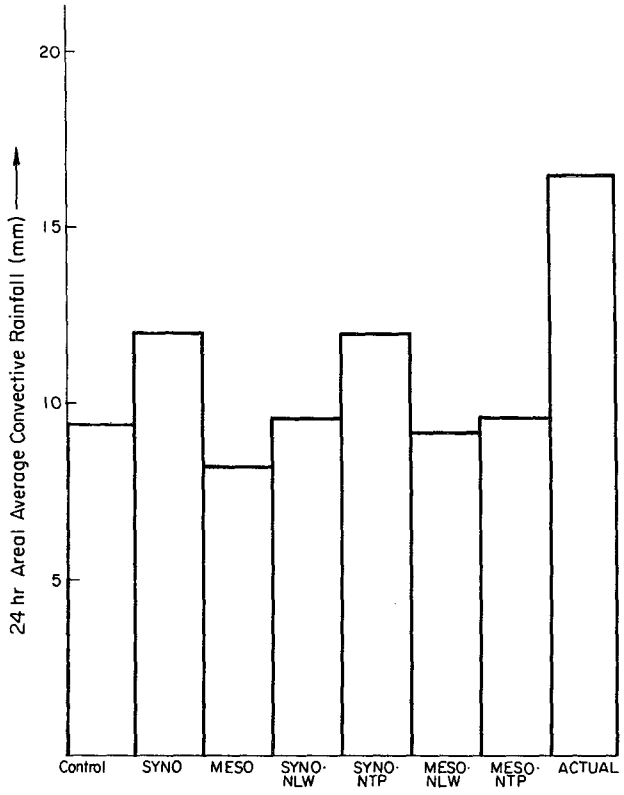

FIG. 16. (*Continued*)

level horizontal velocity convergence resulted in more precipitation over the highlands than the lowlands. There was minimal convective precipitation for the first 7 h of the simulation (Fig. 16a). However, the peak convective rainfall value of 0.72 mm h^{-1} occurred over Kenya in the afternoon at 1100, 1300, 1600, and 1800 LT. The grid-averaged 24-h convective precipitation computed from the predicted model output over the country was 8.2 mm (Fig. 16c). This was lower than the control of 9.4 mm and the actual observed average rainfall value of 16.5 mm.

It is evident from this MESO simulation that the unique complex terrain inhomogeneity over Kenya with the large water bodies (Lake Victoria, Lake Turkana, and the Indian Ocean) along with the strong equatorial insolation generate strong mesoscale circulations with an intense diurnal cycle in temperature, which is reflected in the precipitation pattern over the country.

e. Isolating the impact of the synoptic-scale monsoonal flow on the rainfall over Kenya (SYNO experiment)

In this experiment (SYNO), topography and land–water contrast datasets were excluded from the model simulation initialized with monsoonal winds in order to eliminate the influence of the local forcings (land–sea breeze, lake–land breeze, upslope–downslope winds, mountain waves, etc.). The terrain undulations of the complex topography over Kenya were also considered a local forcing that play a critical role in the modification of the large-scale monsoonal flow pattern.

The wind streamlines at the lowest model level at 23.9 m ASL (Fig. 18) maintained a southeasterly direction, with a strong easterly zonal component during most parts of the simulation. There was little vertical mixing for the first 12 h of the model integration. The maximum vertical velocity (figure not shown) attained during the whole simulation period was 1.0 cm s^{-1}, with subsidence of -2.4 cm s^{-1} at 1600 UTC (1900 LT). The horizontal divergence field (figure not shown) depicted horizontal velocity divergence over

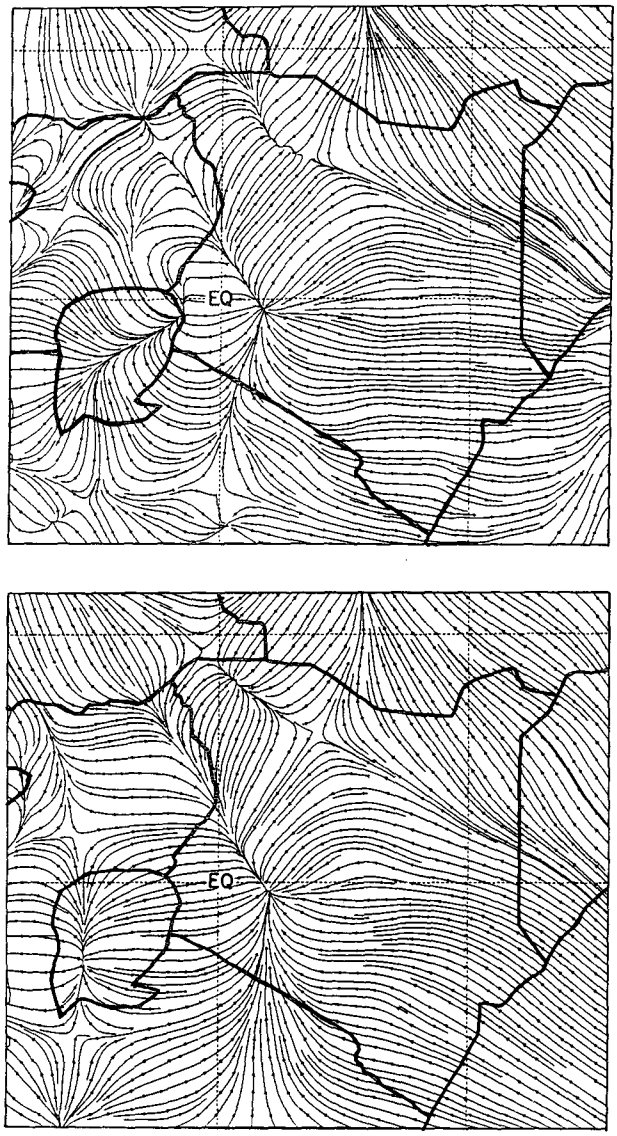

FIG. 17. (a) Simulated wind streamlines at 23.9 m ASL at 0500 UTC (MESO). (b) Simulated wind streamlines at 23.9 m ASL at 1200 UTC (MESO).

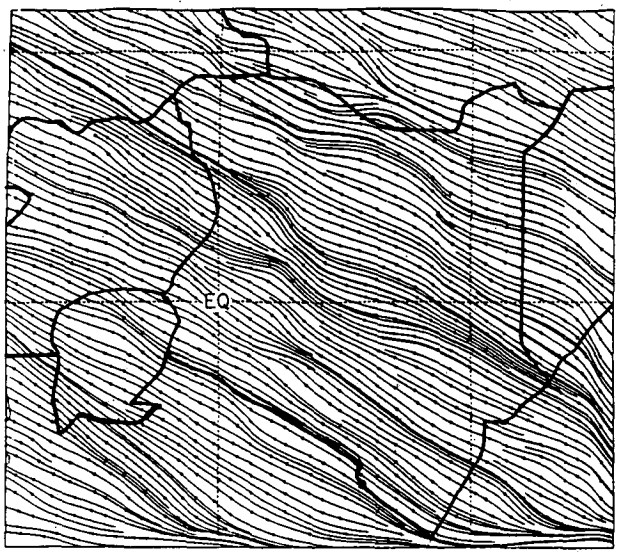

FIG. 18. Simulated wind streamlines at 23.9 m ASL at 1200 UTC (SYNO).

the whole domain for the first 12 h of the simulation and convergence over many portions of the domain during the afternoon. The potential temperature field (figure not shown) depicted warmer temperatures to the east of the domain as compared to the west during the early hours of model simulation. The maximum temperature values in degrees Celsius at 23.9 m ASL increased from 26.3°C at 0100 UTC to 29.3°C at 1200 UTC and remained at 29.0°C up to 1600 UTC, dropping to 28.9°C at 1700 UTC, 28.7°C at 1800 UTC, and 28.6°C at 1900 UTC. These temperatures were almost evenly spread over the domain and the increase was indicative of a buildup of convective instability due to strong solar insolation. The moisture advected into the domain was similarly well spread out almost homogeneously over the country. The maximum value of the moisture simulated was 21.6 g kg^{-1} (at 23.9 m ASL) toward the end of the simulation at 2100 UTC. This was an increment of 5.1 g kg^{-1} from an initial value of 16.5 g kg^{-1} at the same level.

The convective rainfall was caused by the large-scale horizontal velocity convergence that is evident in the regions of local concentration in the low-level monsoonal wind streamlines in Fig. 18. The convective rainfall was mostly confined to the afternoon period (the time of maximum solar insolation and low static stability) and was almost evenly spread out over the country with minimum values close to the eastern boundary of the domain. The maximum convective precipitation value of 3.0 mm h^{-1} was simulated at 1900 LT (Fig. 16a). The 24-h grid-averaged convective precipitation value computed from the predicted model output over Kenya was 12.0 mm, which was above the CONTROL value of 9.4 mm but below the ACTUAL rainfall value of 16.5 mm (Fig. 16c). The convective precipitation pattern and distribution were similarly different from the control.

The occurrence of a significant amount of model-predicted convective rainfall in the SYNO experiment was not anticipated, especially since topography and land–water contrast had been excluded from the simulation and replaced with a flat horizontally homogeneous terrain.

In order to understand why the SYNO experiment generated more convective rainfall than expected, a number of possible factors that cause rain in Kenya have been listed.

1) TOPOGRAPHY

Rainfall anomalies in Kenya or east-central Africa (Kenya, Uganda, and Tanzania) are presumed in part to be due to terrain peculiarities. For instance, the importance of topography in weather and climate in east Africa has been mentioned by previous investigators (e.g., Trewartha 1966) who inferred that if orographic effects were removed, almost the whole of tropical and subtropical eastern Africa would either be dry-subhumid or dry. This is because genuinely humid weather and climate in Kenya has been found to coincide with high elevations, with limited areas at lowlands (e.g., coastal strip and the Lake Victoria region). Terrain-induced upslope and downslope mesoscale drainage winds are attributed to orographic effects of topography (Okeyo 1987). The presence of an orographic trough over central Africa has been linked to the effects of the east African highlands (Semazzi 1980).

2) LARGE WATER BODIES

The large water bodies like Lake Victoria, Lake Turkana, and the Indian Ocean (which washes the 300-mile coastline of Kenya) are responsible for the occurrence of the sea–land-breeze circulation along the shorelines (Okeyo 1987; Fraederick 1972).

3) THE LARGE-SCALE THERMAL CONVECTION

Kenya sits astride the equator (~5°N–5°S) and experiences strong direct solar insolation throughout the year. As a consequence of this insolation, random thermal convective clouds are induced by afternoon heating from below and nighttime radiative cooling from cloud tops (Asnani 1994).

4) THE NE AND SE MONSOONAL CURRENTS

During the equinoxial period in Kenya when rainfall is heaviest (Trewartha 1966; Asnani 1993; Findlater 1968):

(i) the monsoonal airflow has a prevailingly strong easterly zonal component;

(ii) more oceanic moisture is advected landward as a consequence of (i);

(iii) the vertical structure of the atmosphere is less stable because of the presence of the ITCZ.

5) ITCZ

Latitudinally migrating ITCZ follows the course of the overhead sun. The ITCZ favors active large-scale convergence through deep humidification of air that creates conditions that are conducive to rain generation (Johnson 1962; Kiangi et al. 1981).

6) SYNOPTIC-SCALE DISTURBANCES

(i) Observational evidence suggests the existence of well-organized westward-moving extratropical synoptic-scale frontal disturbances that are embedded in the SE monsoonal current and in the near-equatorial trough (e.g., Forsdyke 1949; Okoola 1989; Cadet et al. 1977).

(ii) The presence of eastward-moving waves in the middle and higher troposphere embedded in either easterly or westerly circulations and believed to be induced by low pressure troughs in the higher latitudes (Thompson 1957). These synoptic-scale disturbances activate convection when moisture is adequate, even in the presence of a diffuse ITCZ.

7) FRICTIONAL DRAG

Retardation of monsoonal air current by friction is a factor that may result in large-scale frictional convergence (Asnani 1993).

Factors 1 and 2 give rise to mesoscale systems, whereas factors 3–7 represent the synoptic-scale systems. The mesoscale systems interact with the synoptic-scale systems to release convective instability that results in showers and thunderstorms (Asnani and Kinuthia 1979).

In the SYNO experiment, factors 1 and 2 were excluded from the simulation. This meant that factors 3–7 were still operational.

Therefore, it may be inferred that the cumulative effect of strong solar insolation, the presence of the ITCZ, the monsoonal currents with a strong zonal component at surface level, the synoptic-scale waves over the Indian Ocean embedded in the SE monsoonal current including the midlevel synoptic-scale waves, and the frictional retardation may have caused a buildup of convective instability during the first 12 h of model simulation. The release of convective instability gave rise to sudden active convection during the afternoon period. This resulted in the temporal and spatial pattern of precipitation rain that was substantially different from the observed (ACTUAL) and the CONTROL.

Conversely, an alternative and probably more plausible explanation for the unexpected active weather in the SYNO experiment is as follows. The sudden removal of topography and suppression of land–water contrast may not necessarily result in the elimination of orographic effects immediately since significant imbalances may develop in the model with the result that what is observed during the first 24 h of simulation merely reflects the adjustment process toward a new quasi-equilibrium state. Therefore, the increment in the SYNO rainfall could be attributed to the significant imbalances that may have developed during the adjustment process in the model to a new quasi-balanced state.

7. Additional sensitivity experiments

Four additional sensitivity studies were performed to determine (i) the role played by the large water bodies of Lake Victoria, Lake Turkana, and the Indian Ocean on the convective precipitation over Kenya in the absence of large-scale monsoonal winds and topography (MESO.NTP); (ii) the impact of orographic winds on convective rainfall in the absence of the monsoonal flow and the water bodies (MESO.NLW); (iii) the combined impact of large water bodies and monsoonal winds on convective rainfall in the absence of mountains (SYNO.NTP); and (iv) the combined impact of orographic winds and monsoonal winds on convective rainfall in the absence of large water bodies (SYNO.NLW). The results of these experiments are illustrated in Figs. 16b and 16c.

The main conclusion from this set of sensitivity experiments is that while convective precipitation patterns can vary substantially when one of the forcing mechanisms is removed (i.e., land–water contrast, terrain, monsoonal flow), the country's 24-h averaged convective precipitation is relatively insensitive to the removal. Without one or more of the forcings, the daytime insolation creates convective instability, which is eventually released by one or more of the remaining forcing mechanisms.

8. Conclusions

- This study showed that finescale horizontal and vertical resolution in the model was beneficial in the forecast of the low-level monsoonal wind fields, including the location and intensity of convective precipitation over Kenya. This was due to the capability of the model in capturing small-scale details of orography and in responding to the land–water contrast, both of which induce strong mesoscale systems with an intense diurnal cycle. However, it was felt that use of a 5′ topography dataset together with a finer spatial resolution (e.g., 10 km) would better simulate the time, location, and intensity of the convective precipitation over the country.
- A large fraction of the moisture available for condensation over Kenya originated from the Indian Ocean. The moisture was transported by the shallow low-level monsoonal winds from the Indian Ocean into the ITCZ.
- The resultant diurnal precipitation pattern was a consequence of the nonlinear interaction between the monsoonal winds and the mesoscale circulations gen-

erated by the large water bodies and orography. The mesoscale 24-h grid-averaged convective precipitation value computed from the predicted model output over Kenya with a value of 8.2 mm was less than the CONTROL of 9.4 mm and the ACTUAL observed areal average rainfall of 16.5 mm computed from autographic records for 24 stations in Kenya.

- The purely monsoonal convective rainfall value (SYNO) of 12.0 mm showed that the somewhat meridionally oriented orography moderates rainfall in Kenya by impeding the westward inland penetration of a substantial amount of moisture-laden but shallow monsoonal winds.
- Conversely, the registered increment in the modeled SYNO rainfall could simply have been triggered by significant imbalances that may have developed in the model during the adjustment of the model to a new quasi-balanced state owing to the sudden removal of topography and land–water contrast from the model.
- Without topography (but with land–water contrast, SYNO.NTP) it would be possible to have more convective precipitation. This precipitation would, however, be confined mostly to the areas between Lake Victoria, Lake Turkana, and the Indian Ocean with very little precipitation over the large water bodies themselves.
- The sensitivity experiments showed that the complex terrain irregularities and the large water bodies over Kenya generate individual mesoscale systems with an intense diurnal cycle over the country. The mesoscale circulations interact among themselves and also cause variations in the intensities of the large-scale monsoonal flow. These nonlinear interactions were reflected in the various precipitation amounts and patterns over the model domain.
- The overall performance of the RAMS in realistically replicating the low-level monsoonal winds, the mid- and upper-level flows, the ITCZ position, the east African low-level jet (EALLJ), and the mesoscale circulations of the atmosphere over Kenya was good. The model's performance in forecasting quantitative precipitation was found to be fair in general since the model-predicted 24-h grid-averaged convective precipitation value of 9.4 mm (CONTROL) was 57% of the actual observed areal average rainfall of 16.5 mm (ACTUAL) for 24 stations over Kenya.

Acknowledgments. This paper was part of the first author's Ph.D. work, which he carried out under the tutelage and astute guidance of the second author while visiting Colorado State University. The authors would like to bestow their gratitude to Professor L. J. Ogallo and to the late Professor A. E. Okeyo, both of the University of Nairobi, for their invaluable advice and suggestions in the course of this research. Many thanks go to the World Meteorological Organization (WMO) for offering the first author an 18-month fellowship enabling him to perform computing work for this research at CSU. Thanks to the United States Agency (Nairobi) and WMO for providing Joseph Mukabana with a round-trip air ticket and to the University of Nairobi for granting study leave. Roger Pielke acknowledges the support of Professor L. J. Ogallo to visit Kenya for a period of time in the summer of 1988. The insight into weather patterns over east Africa and valuable discussions with scientists at the University of Nairobi, the Institute of Meteorological Training and Research (at the Kenya Meteorological Department), and other African scientists attending the meeting is also acknowledged. This research was supported in part by the National Science Foundation (NSF) Grants ATM-89-15265 and ATM-9306754.

NCAR provided computing resources on the CRAY Y-MP8/864 supercomputer and the global ECMWF pressure-level data, NMC rawinsonde and surface observation datasets, global topography, and global sea surface temperature datasets required for this study. Thanks to the Kenya Meteorological Department for providing observational data used for model verification. The authors are grateful for the invaluable help and advice in setting up RAMS from Drs. Bob Walko, John Lee, and the affable Joseph Eastman, all at the Department of Atmospheric Science at Colorado State University. Last, but not least, many thanks go to Bryan Critchfield and Dallas McDonald for the excellent work done in preparing this manuscript.

REFERENCES

Asnani, G. C., 1993: *Tropical Meteorology,* Vol. 1 and Vol. 2. Indian Institute of Tropical Meteorology, 1202 pp.

——, and J. H. Kinuthia, 1979: Diurnal variation of precipitation in East Africa. Kenya Meteorological Department, Research Report No. 8/79, 1–58.

Bannon, P. R., 1979a: On the dynamics of the East African jet. Part I: Simulation of mean conditions for July. *J. Atmos. Sci.,* **36,** 2139–2152.

——, 1979b: On the dynamics of the East African Jet. Part II: Jet transients. *J. Atmos. Sci.,* **36,** 2153–2168.

Barnes, S. L., 1973: Mesoscale objective map analysis using weighted time-series observations. NOAA Tech. Memo. ERL NSSL-62, National Severe Storms Laboratory, Norman, OK, 38 pp.

Beltrando, G., 1990: Space–time variability of rainfall—April and October–November over East Africa during the period 1932–1983. *Int. J. Climatol.,* **10,** 691–702.

Bougeault, P., 1992: Current trends and achievements in limited area models for numerical weather prediction research. WMO/TD No. 510. Programme on Weather Prediction Research (PWPR). Report Series No. 3.

Cadet, D. L., and P. Olory-Togbé, 1977: The propagation of tropical disturbances over the Indian Ocean during the summer monsoon. *Mon. Wea. Rev.,* **105,** 700–708.

Chen, C., and W. R. Cotton, 1983: A one-dimensional simulation of the stratocumulus capped mixed layer. *Bound.-Layer Meteor.,* **25,** 289–321.

Clark, T. L., and R. D. Farley, 1984: Severe downslope windstorm calculations in two and three spatial dimensions using anelastic interactive grid nesting: A possible mechanism for gustiness. *J. Atmos. Sci.,* **41,** 329–350.

Davies, H. C., 1976: A lateral boundary formulation for a multi-level prediction model. *Tellus,* **102,** 405–418.

Findlater, J., 1968: The month-to-month variation of mean winds at low levels over East Africa. Tech. Memo. No. 12, Nairobi, Kenya. East African Meteorological Department.

——, 1972: Aerial exploration of the low level cross-equatorial current over East Africa. *Quart. J. Roy. Meteor. Soc.,* **98,** 274–289.

Forsdyke, A. G., 1944: Synoptic analysis in the western Indian Ocean. *EAMD.* Memoirs II, No. 3.

——, 1949: Weather forecasting in tropical regions. Great Britain Meteorological Office. *Geophys. Mem.,* **X,** No. 82, 32.

Fraederick, K., 1972: A simple climatological model of the dynamics and energetics of the nocturnal circulation at Lake Victoria. *Quart. J. Roy. Meteor. Soc.,* **98,** 332–335.

Johnson, D. H., 1962: Rainfall in East Africa. *Quart. J. Roy. Meteor. Soc.,* **88,** 1–19.

Kiangi, P. M. R., M. M. Kavishe, and J. K. Patnaik, 1981: Some aspects of the mean tropospheric motion field in East Africa during the long-rains season. *Kenya Science and Technology Series,* **A2,** 91–103.

Kinuthia, J. H., 1992: Horizontal and vertical structure of the Lake Turkana jet. *J. Appl. Meteor.,* **31,** 1248–1274.

Klemp, J. B., and R. B. Wilhelmson, 1978: The simulation of three-dimensional convective storm dynamics. *J. Atmos. Sci.,* **35,** 1070–1096.

Kuo, H. L., 1974: Further studies of the parameterization of the effects of cumulus convection on large-scale flow. *J. Atmos. Sci.,* 1232–1240.

Messinger, F., and A. Arakawa, 1976: Numerical methods used in atmospheric models. GARP Publication Series, No. 14, WMO/ICSU Joint Organizing Committee, 67 pp.

Molinari, J., 1985: A general form of Kuo's cumulus parameterization. *Mon. Wea. Rev.,* **113,** 1411–1416.

Okeyo, A. E., 1987: The influence of Lake Victoria on the convective activities over the Kenya highlands. *J. Meteor. Soc. Japan,* Special volume, 689–695.

Okoola, R. E. A., 1989: Westward moving disturbances in the southwest Indian Ocean. *Meteor. Atmos. Phys.,* **41,** 35–44.

Pielke, R. A., 1984: *Mesoscale Meteorological Modeling.* Academic Press, Inc., 612 pp.

——, W. R. Cotton, R. L. Walko, C. J. Tremback, M. E. Nicholls, M. D. Moran, D. A. Wesley, T. J. Lee, and J. H. Copeland, 1992: A comprehensive meteorological modeling system—RAMS. *Meteor. Atmos. Phys.,* **49,** 69–91.

Ramage, C. S., 1971: *Monsoon Meteorology.* Academic Press, 296 pp.

Semazzi, F. H. M., 1980: Stationary barotropic flow induced by mountains over the tropical belt. *Mon. Wea. Rev.,* **108,** 922–930.

Thompson, B. W., 1957: Some reflections on equatorial and tropical forecasting. EAMD Tech. Memo., No. 7.

Tremback, C. J., 1990: Numerical simulation of a mesoscale convective complex: Model development and numerical results. Atmospheric Science Paper No. 465, Colorado State University, Fort Collins, CO.

——, and R. Kessler, 1985: A surface temperature and moisture parameterization for use in mesoscale numerical models. Preprints, *Seventh AMS Conf. on Numerical Weather Prediction,* Montreal, PQ, Canada, Amer. Meteor. Soc., 355–358.

——, J. Powell, W. R. Cotton, and R. A. Pielke, 1987: The forward in time upstream advection scheme: Extension to higher orders. *Mon. Wea. Rev.,* **115,** 540–555.

Trewartha, G. T., 1966: The world's problem climates. *Quart. J. Roy. Meteor. Soc.,* **102,** 639–653.